Gaseous Emissions Results from a Three-Cup Flametube Test of a Third-Generation Swirl-Venturi Lean Direct Injection Combustion Concept

Kathleen M. Tacina*, Derek P. Podboy†
NASA Glenn Research Center, Cleveland, Ohio, 44135

Phil Lee† and Bidhan Dam‡
Woodard FST, Zeeland, Michigan, 49464

This paper presents gaseous emissions results from flametube tests of a low-NO_x aircraft gas turbine engine combustor concept. The low-NO_x combustor concept is a third-generation swirl-venturi lean direct injection (SV-LDI-3) design. It was developed to meet the NASA Advanced Air Transport Technology project goals: the development of a combustor suitable for a small-core engine with NO_x emissions 80% below the CAEP/6 standard. Flametube testing showed this design would meet the project goals, with a NO_x reduction estimated to be 85%-89% with respect to CAEP/6.

I. Introduction

NASA has had a continuing effort to reduce the emissions of the oxides of nitrogen (NO_x) from aircraft engines. NO_x has a detrimental effect on the environment both at ground level and at altitude. At ground level, NO_x contributes to smog and ozone. In addition, at supersonic cruise altitudes, NO_x destroys the protective ozone layer.

Therefore, NASA has sustained programs to reduce aircraft engine NO_x emissions. Continued work is needed because aircraft engine advancements designed to increase engine efficiency — and thus reduce carbon dioxide emissions — tend to increase NO_x emissions. In particular, one way to increase engine efficiency is to increase the operating pressure ratio (OPR). However, increasing the OPR increases the combustor inlet temperature and pressure. This increased combustor inlet temperature and pressure will increase NO_x emissions unless the combustor technology is improved.

Currently, NASA has a goal of reducing NO_x emissions by 80% relative to the CAEP/6 standard.[?,?] This goal is supported by the Advanced Air Transport Technology (AATT) project, which focuses on a small-core engine.

To meet the AATT NO_x reduction goals, multiple combustor technologies are being evaluated.[?] One combustor technology is lean direct injection (LDI). In particular, swirl-venturi (SV) LDI. LDI is a fuel-lean combustion concept: all combustion air enters through the dome. In addition, in SV-LDI, multiple small fuel-air mixers replace one traditionally-sized fuel air mixer. Using multiple small fuel-air mixers promotes rapid and uniform fuel-air mixing; this minimizes local near-stoichiometric regions that produce high NO_x emissions.

In the original, first-generation SV-LDI combustor concepts, each fuel-air mixer was the same size (see Figure 1a) and had a simplex fuel injector. These first-generation SV-LDI combustor concepts demonstrated low NO_x emissions.[1] Unfortunately, first-generation SV-LDI had poor low-power operability, even when fuel

*Aerospace Engineer, Combustion Branch
†Engineer, AIAA member
‡Engineer

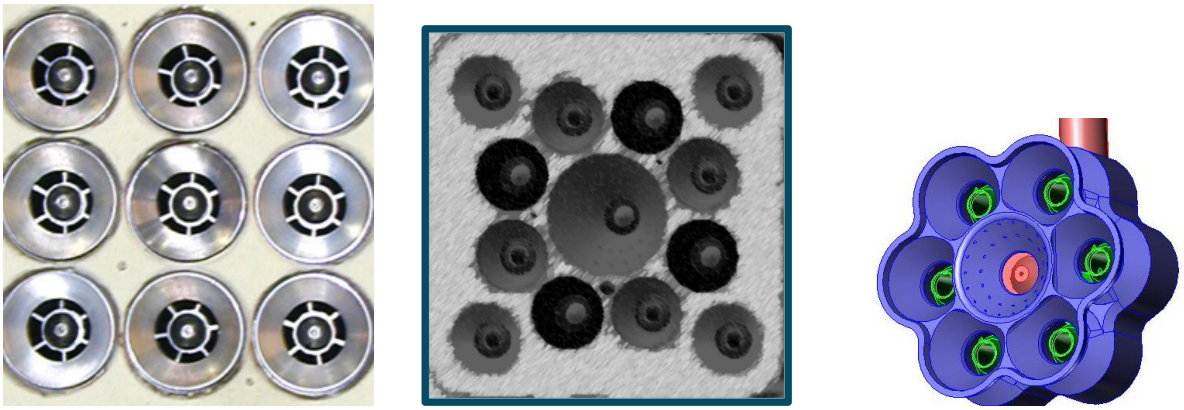

(a) *(b)* *(c)*

Figure 1: *(a) First-, (b) second-, (c) and third-generation LDI configurations.*

staging was used to fuel only some of the fuel-air mixers.[1] In addition, because a fuel line went to each fuel-air mixer, there were concerns about thermal management of the fuel and fuel line complexity.

Second-generation SV-LDI combustor concepts were designed to further reduce NO_x while also improving low-power operability. To further reduce NO_x, some of the simplex fuel injectors used in first-generation SV-LDI designs were replaced by airblast fuel injectors. To improve low-power operability, a large pilot fuel-air mixer with an extended venturi was added. Three second-generation SV-LDI configurations were tested; a representative configuration is shown in Figure 1b. Testing showed that the second-generation SV-LDI configurations had reduced NO_x emissions compared to the baseline first-generation SV-LDI configuration. In addition, the second-generation SV-LDI configurations had good low-power operability.[2,3]

Like second-generation SV-LDI concepts, third-generation SV-LDI combustor concepts were designed to continue to reduce NO_x emissions and have good low-power operability. The design of third-generation SV-LDI fuel-air mixers is similar to that of second-generation SV-LDI fuel-air mixers, as shown in Figure 1c. Thus, third-generation SV-LDI combustor designs are expected to have low NO_x emissions and good low-power operability.

In addition, third-generation SV-LDI combustor concepts were designed to reduce fuel line complexity and improve the thermal management of the fuel. The fuel stems of second- and third-generation SV-LDI concepts are compared in Figure 2. The second generation fuel stem branches out to multiple (13) fuel lines and injectors. Each fuel line feeds an injector in a fuel-air mixer; hence, 13 injectors for 13 fuel-air mixers. In contrast, the third-generation fuel stem has a single injector with multiple injection points; hence one injector for multiple fuel-air mixers. This reduces the fuel line complexity and concerns with the thermal management of the fuel.

This paper reports the NO_x and CO emissions of the 3-cup third-generation SV-LDI flametube tests. Emissions are compared to second-generation LDI configurations as well as to AATT emissions goals.

II. Experimental Hardware and Facilities

A. LDI Hardware

The third-generation SV-LDI combustor concepts were developed for a small-core engine as part of NASA's Advanced Air Transport Technology (AATT) project. This small core requires the fuel-air mixers to be tightly packed. To accomplish the tight packing, adjacent cups are not identical. Instead, 7-point cups (a pilot surrounded by 6 main fuel-air mixers) alternate with 5-point cups. A 5-cup sector is shown in Figure 3.

Since each cup is not identical, the flametube tests are done with multiple cups instead of a single cup. Therefore 3-cup sector will be tested in the CE-5 medium pressure flametube. The 3-cup sector is composed of two 7-point cups and one 5-point cup, as shown in Figure 4.

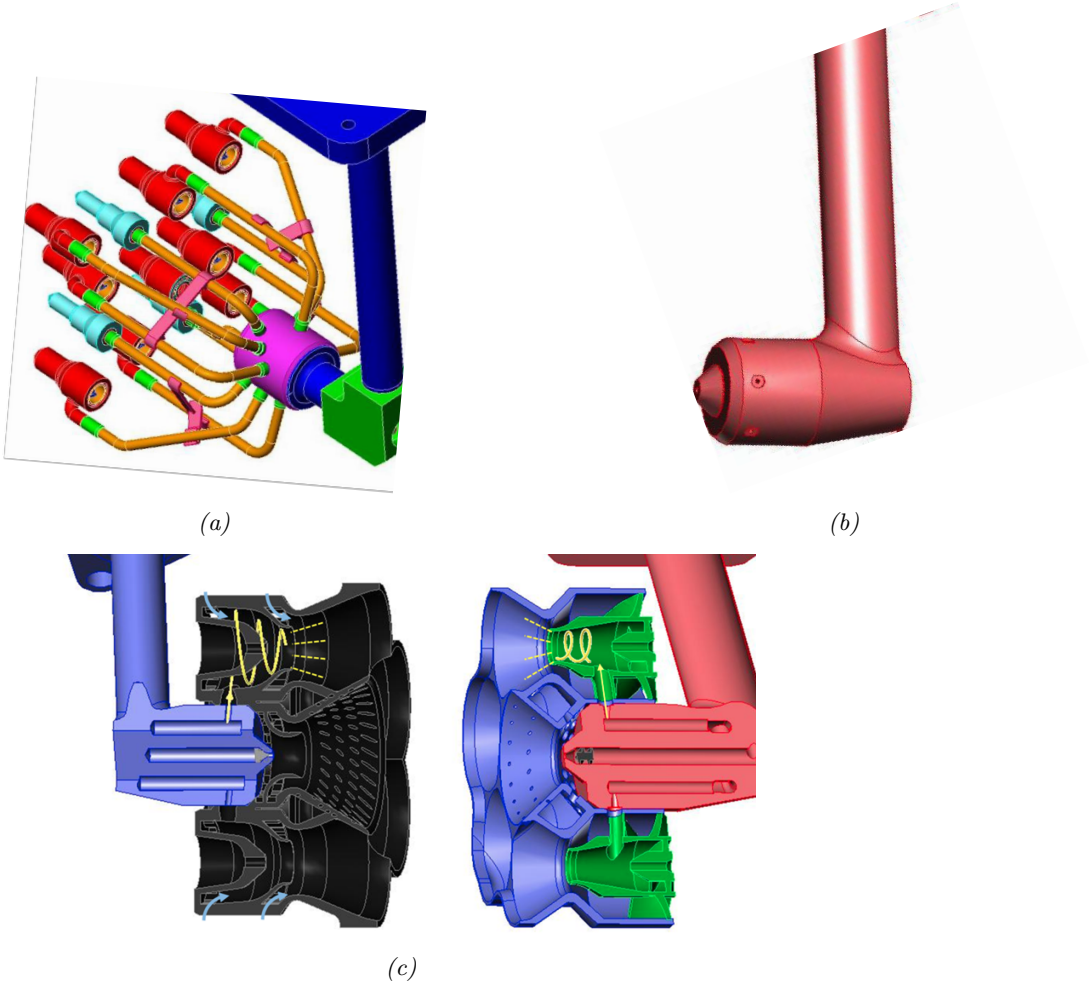

(a) *(b)*

(c)

Figure 2: *(a)Second- and (b, c) third-generation LDI fuel stems.*

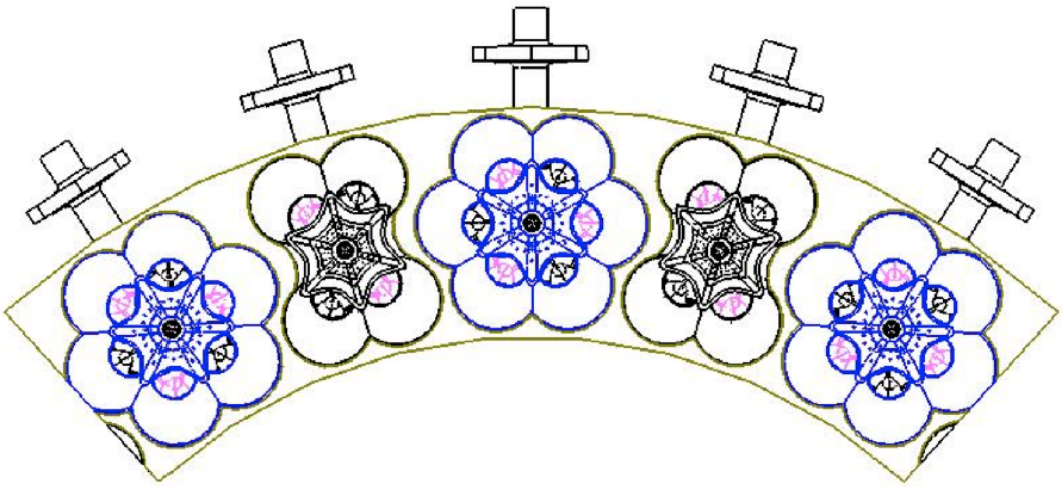

Figure 3: *A third-generation SV-LDI 5-cup sector.*

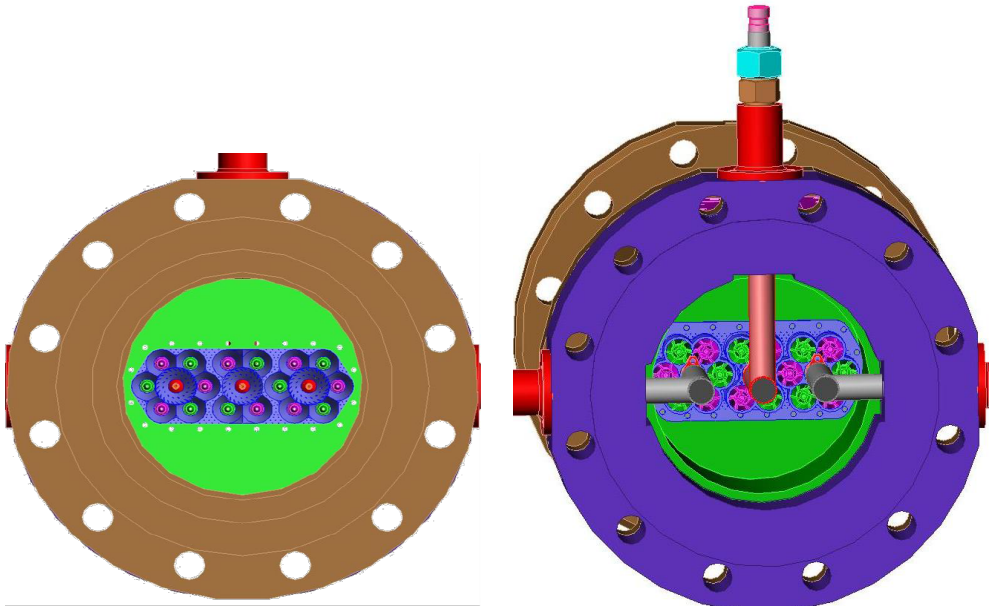

(a) *(b)*

Figure 4: *The three-cup third-generation LDI flametube hardware. Shown are (a) downstream looking upstream and (b) upstream looking downstream.*

B. CE-5 Medium Pressure Flametube

These tests were done in the CE-5 intermediate pressure combustion facility flametube at NASA Glenn Research Center. A sketch of a flametube is shown in Fig. **??**. The flametube has a cast ceramic liner. This facility can supply nonvitiated air preheated to 1200 F at pressures up to 275 psia. The test rig is designed to support up to three fuel circuits.

Three fuel circuits were used for testing. The first fuel circuit fed all three center pilot fuel-air mixers. The second circuit fed the four main fuel-air mixers on the center 5-point cup: these four fuel-air mixers are called the "main 1" stage.

The third fuel circuit varied. For all testing except for the 30% ICAO power condition, the third fuel circuit fed all 12 main fuel-air mixers on the two outer 7-point cups. These 12 fuel-air mixers comprise the "main 2" and "main 3" fuel stages. The main 2 stage is made up of the inner 3 fuel-air mixers on each of the 7-point cups, for a total of 6 fuel-air mixers. The main 3 stage is made up of the 3 outer fuel-air mixers on each of the 7-point cups. For the 30% power ICAO point, the third fuel circuit fed only the main 2 stage.

C. Steady-State Data Acquisition and Processing

Steady-state data was acquired at a rate of 1 Hz using the NASA Glenn ESCORT real-time data acquisition system. It recorded facility conditions such as temperature and pressure as well as gaseous emissions.

Gaseous emissions were measured using a 5-hole probe connected to a gas bench. The 5 holes were spaced 2-cm apart. All 5 holes were on the centerline of the combustor, and the center hole line up with the center pilot.

The gas bench followed the SAE ARP-1255D[4] standard, except that unburned hydrocarbon (UHC) measurements were unavailable for this test. Post-processing followed the SAE ARP-1533B[5] standard. Adiabatic flame temperatures are calculated using the Chemical Equilibrium for Applications (CEA) equilibrium code.[6,7]

1. Fuel-air ratio: metered vs. gas analysis

The equivalence ratio ϕ calculated from the gas analysis results was compared to the equivalence ratio calculated from the metered fuel and air flow rates. Except at 30% power conditions, the equivalence ratios

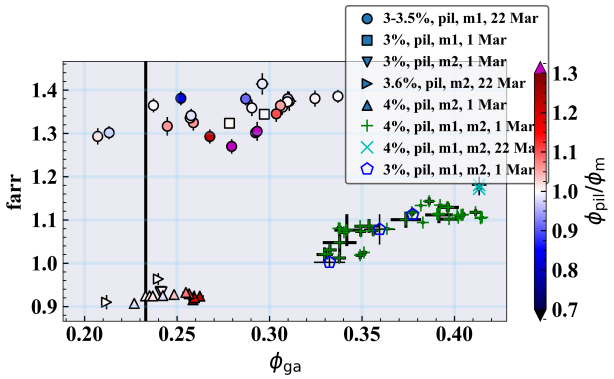

Figure 5: *30% power ICAO point results: The fuel-air ratio from gas analysis compared to the fuel-air ratio from fuel metering (farr), as a function the the equivalence ratio obtained from gas analysis, ϕ_{ga}. The farr is much farther from 1.0 than is typical, due to unrepresentative gas sampling with the fuel staging schemes used for the 30% power point. For all other test conditions, farr was very close to 1.0*

calculated by both methods are close, typically within 5%.

For the 30% ICAO power point, the fuel air ratios calculated by gas analysis and by fuel metering were not close, and varied with the fuel staging. This is shown in Figure 5, which shows the ratio of fuel-air from gas analysis to fuel-air from metering (farr). When only the pilot and main 1 stages are on, gas analysis gives a much higher fuel-air ratio than the metered value. When the pilot, main 1, and main 2 stages are on, gas analysis gives a somewhat higher fuel-air ratio than the metered value. When the pilot and main 2 stages are on, gas analysis gives a slightly lower fuel-air ratio than the metered value. This is due to unrepresentative sampling at these conditions. Using multiple multi-hole probes would give better sampling. However, muliple water-cooled probes would provide too much blockage. For future testing, we will consider expanding the casting area downstream of the combustion section, which may allow us to install additional probes.

For the 30% power ICAO point[a], all emissions estimates are based on the fuel-air ratio obtained from gas analysis. The reason is that a point with a fuel-air ratio higher than the metered value indicates the gas sample itself sampled combustion products with a higher fuel-air ratio. Such a sample would be expected to have a higher NO_x than the average across the entire flametube. Similarly, a sample with a lower than metered fuel-air ratio will probably have a lower NO_x concentration. Using the fuel-air ratio from gas analysis instead of the metered value partially compensates for this effect.

D. NASA N+3 small core cycle

III. Results

A. Evaluation of ICAO NO_x emissions

This section evaluates the NO_x emissions at the ICAO conditions. The combustor conditions at the ICAO conditions are shown in Table 1.Note that in an actual engine, some of the combustor air is used to cool the combustor liner, increasing the local fuel-air ratio in the combustion zone. However, there is no liner cooling in the CE-5 flametube: the combustion zone is surrounded by a ceramic casting. To compensate for this, the fuel-air ratio is increased in CE-5 testing. It is assumed that 20% of the combustor air is used for liner cooling, and so the flametube fuel-air ratios are increased by $\frac{1}{0.8} = 1.25$.

The emissions at the 7% and 30% ICAO conditions are evaluated directly. However, the CE-5 flametube cannot reach the pressures for the 85% and 100% power ICAO conditions. As Table 1 shows, the combustor pressure at the 100% ICAO point is 38.0 bar and the pressure at the 85% ICAO point is 32.7

[a]and every other point, altough it only makes a big difference at 30%

Table 1: *NASA N+3 small-core cycle, giving the combustor inlet pressure p_3, combustor inlet temperature T_3, and combustor equivalence ratio ϕ_{eng}. Twenty percent combustor liner cooling is assumed to calculate the flametube equivalence ratio ϕ_{ft} and flametube combusted gas temperature T_{ft}*

Condition	p_3 (MPa)	T_3 (K)	ϕ_{eng}	ϕ_{ft}	T_{ft} (K)
7% ICAO	0.71	553	0.103	0.128	890
30% ICAO	1.41	661	0.186	0.233	1,231
85% ICAO	3.28	835	0.325	0.402	1,727
100% ICAO	3.80	870	0.354	0.442	1,832
Cruise	1.83	827	0.392	0.490	1,887
Top of Climb	1.95	834	0.377	0.471	1,858
Rolling Takeoff	4.43	957	0.446	0.558	2,107

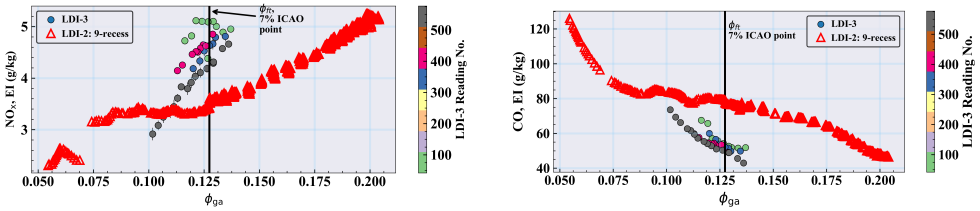

(a) *(b)*

Figure 6: *7% power ICAO point: (a) NO_x and (b) CO emissions plotted against the equivalence ratio obtained from gas analysis, ϕ_{ga}.*

bar. However, as stated in section **??**, the CE-5 Stand 1 flametube can only reach approximately 18.6 bar. Therefore, correlation equations are developed and used to estimate NO_x emissions at the 100% and 85% power conditions.

1. 7% power

Figure 6 shows the NO_x and CO emissions at the 7% power condition. At this condition, only the pilot fuel circuit is on. At the 7% equivalence ratio of 0.127, the NO_x emissions index is 4.3 g/kg and the CO emissions index is 51 g/kg. Assuming the UHC emissions index is 1/3 that of CO, the combustion efficiency is 97%. This combustion efficiency is lower than desired but acceptable.

The 7% power condition was repeated on four test days. Unfortunately, as shown in Figure 6, both the NO_x and CO emissions varied with the test day. Except for the NO_x curve on the first day of testing,[b], the NO_x and CO emissions on each day fall on a single curve. The curves are reasonable with NO_x increasing and CO decreasing as the equivalence ratio increases. However, the curves are slightly different each day. It is unclear why this is the case. One possibility is that fuel-air mixing was actually different on each day. During testing, small cracks appeared in the pilot venturis[c]. These cracks would not have significantly the fraction of air going to the pilot stage. However, they may have changed the fuel-air mixing slightly, resulting in different curves for NO_x and CO emissions[d]. For the ICAO NO_x emissions, the curves for the last day of testing were used.

[b]On the first test day, the NO_x emissions curve is flat. This indicates that there may be problems with the NO_x analyzer at these points.

[c]Although cobalt-chrome material used to manufacture the LDI hardware is a high temperature material, it ductility is not as good as the high temperature stainlesss steel used to manufacture the LDI-2 hardware. In the future, a different material may be used or the thickness of the pilot venturis may be increased.

[d]For other power conditions, there was no effect of testing date: emissions were the same (within typical scatter) for data taken at the same point on different days. This is shown in the plots for the 30% power ICAO point. Emissions were also checked at some high power conditions, although the results are not shown.

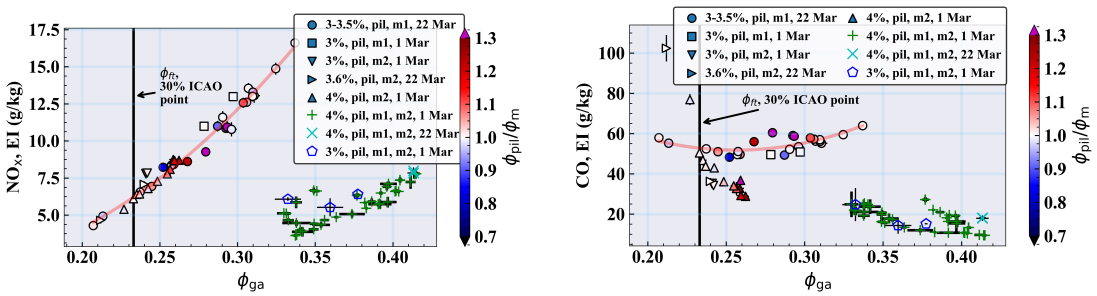

Figure 7: *30% power ICAO point: (a) NO_x and (b) CO emissions plotted against the equivalence ratio obtained from gas analysis, ϕ_{ga}.*

Figure 6 also compares the emissions to those of the LDI-2 9-recess design. LDI-3 has higher NO_x emissions and lower CO emissions. In addition, both the NO_x and CO curves are steeper for LDI-3. There may be two reasons for this. First, the air splits between the pilot and main fuel-air mixers are different for LDI-2 and LDI-3. Second, the 9-recess LDI-2 configuration had an airblast fuel injector on the pilot whereas LDI-3 has a simplex fuel injector; in LDI-2, airblast tips were shown to have lower NO_x emissions but higher CO emissions.[8] Increasing the percentage of air going to the pilot could potentially decrease NO_x emissions at 7% power.

B. 30% power

Figure 7 shows the NO_x and CO emissions at the 30% power conditions. This was the only problematic condition for the LDI-3 design. At 30%, not only was the farr off (see section 1), but it was hard to find a "good" fuel staging.

The 30% dome equivalence ratio of 0.233 could not be reached with all fuel stages on. It furthermore could not be reached with only the main 3 stage off (i.e., with only the pilot, main 1, and main 2 stages on). This equivalence ratio could be reached with the pilot and only one main stage on. The NO_x emissions index was 6.25 g/kg and the CO emissions index was approximately 50 g/kg. Again assuming the the UHC emissions index is 1/3 that of CO, the combustion efficiency is 97.2%.

Neither the NO_x emissions nor the combustion efficiency is good for the 30% point. As with the 7% power point, increasing the percentage of air going to the pilot cup would decrease NO_x emissions. Emissions at the 30% power point would also be lower if the equivalence ratio was increased enough to allow at least two of the three main stages to be fueled. For example, the NO_x and CO emissions would be lower and the combustion efficiency higher if the older UEET large engine cycle or UEET regional engine cycle was used.[1]

C. High power conditions

At the high power conditions, the CE-5 flametube could not reach the correct combustor inlet pressures. Therefore, correlation equations are used to estimate the NO_x emissions.

The data used for the correlation equations is shown in Figure 8. The data is clustered near following conditions: the inlet temperature for 85% power, the inlet temperature at 100% power, and the PC90 supersonic cruise condition (from a supersonic cycle.) Additional data was taken at other conditions to provide a wider variety of conditions for the correlation equations. Typically, this other data was taken as the inlet temperature was being adjusted. The inlet temperature changed slowly, so the variation during a 1-minute sample was small.

1. CO emissions and combustion efficiency

At these conditions, the CO emissions are low and the combustion efficiency is high, typically above 99.99%. Figure 9a compares the measured CO emissions with the equilibrium CO emissions as calculated by the CEA chemical equilibrium program. The measured CO emissions are slightly above the equilibrium CO.

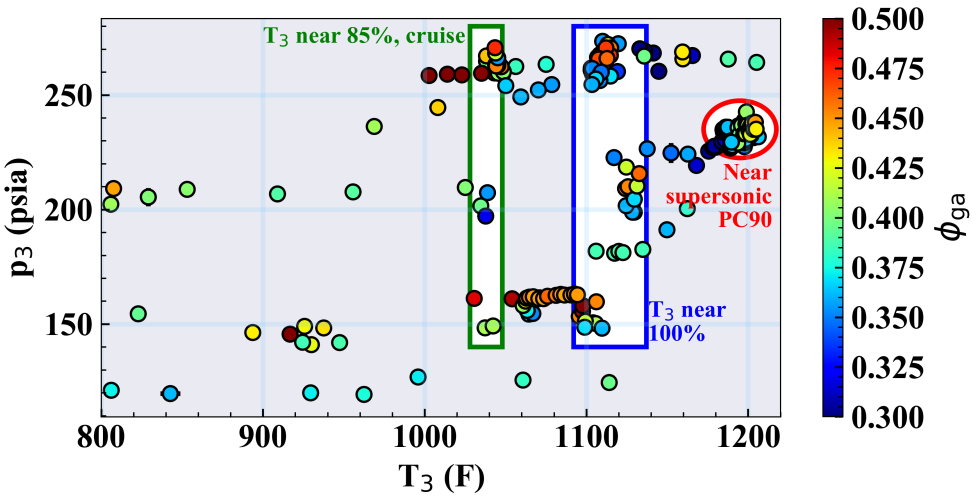

Figure 8: *Inlet temperature T_3 and inlet pressure p_3 used to evaluate emissions at high power conditions.*

The equilibrium CO emissions are then subtracted from the measured CO emissions to give the "corrected CO" emissions. The corrected CO emissions are then used to calculate the combustion efficiency[e]. Since the UHC are not measured, the combustion efficiency is calculated using two different assumptions for the UHC: (1) the UHC emissions index is 1/3 of the corrected CO emissions index and (2) there is no UHC. Based on LDI-2 results, the second assumption — no UHC — is probably closer to correct. Except at the highest flame temperatures, combustion efficiency is typically above 99.99%, as shown in Figure 9b.

2. ICAO NO_x emissions and correlation equations

The NO_x emissions for most of the data used to calculate the correlation equations is shown in Figure 10. The legend shows 36 different curves. However, most of the data is taken at only a few conditions, as shown previously in Figure 8. The purpose of Figure 10 is to provide a visual summary of the NO_x emissions.

Individual curves are shown later in Figures 11-**??**. These curves are arranged in the following order. First, curves at constant inlet pressure are shown, starting with the highest inlet pressure. For a given inlet pressure, there are shown, in order, comparisons showing the effect of inlet temperature, comparisons showing the effect of combustor pressure drop, and comparisons with LDI-2. Finally, curves at a constant inlet temperature but varying inlet pressure are shown.

Before calculating correlation equations, Figures 10 and 11 are used to roughly estimate the NO_x emissions at the 85% and 100% ICAO power conditions. At 85% power, the dome adiabatic flame temperature is 1725 K. From Figures 10 and 11a, the NO_x emissions are approximately 5 g/kg at 260 psia and an air pressure drop of 4%. Assuming that NO_x emissions increase with $p^{0.5}$ to $p^{0.6}$, NO_x emissions at 85% power are estimated to be roughly 6-7 g/kg. Similarly, using Figures 10 and 14b, NO_x emmissions are about 10.5 g/kg at 260 psia and so should be roughly 15-17 g/kg at 100% power, 552 psia.

The form of the correlation equations used for estimating NO_x is taken from the forms developed for LDI-1 and LDI-2.[1–3] The form of the correlation equations is:

$$\mathrm{NO}_x,\ \mathrm{EI} = p_3^a e^{(T_3/b)} \Delta p^c \left[d_p e^{(T_{\mathrm{ad,\ p}}/e_p)} + d_m e^{(T_{\mathrm{ad,\ m1}}/e_m)} + d_m e^{(T_{\mathrm{ad,\ m2}}/e_m)} + d_m e^{(T_{\mathrm{ad,\ m3}}/e_m)} \right], \qquad (1)$$

where the combustor inlet temperature p_3 is in bars, the combustor inlet temperature T_3 is in Kelvin, the air pressure drop Δp is in percent of p_3, and the adiabatic flame temperature T_{ad} is in Kelvin. The subscripts p

[e]Subtracting the equilibrium CO from the meausured CO is necessary to prevent the combustion efficiency from decreasing as flame temperature increases. For example, at a pressure of 300 psia and an equivalence ratio of 0.4, the CO emissions index is 70% higher at an inlet temperature of 1000 F than it is at 1200 F. With no correction for the equilibrium CO, this would mean that the combustion efficiency is lower at 1200 F than it is at 1000 F. This is not a physically meaningful result. It is assumed that the CO will be converted to CO_2 before the engine exit plane. Also note that, due to the lower pressure, the CO emissions index is higher in the CE-5 flametube tests than it would be at the correct inlet pressure. This is discussed in more detail in[3]

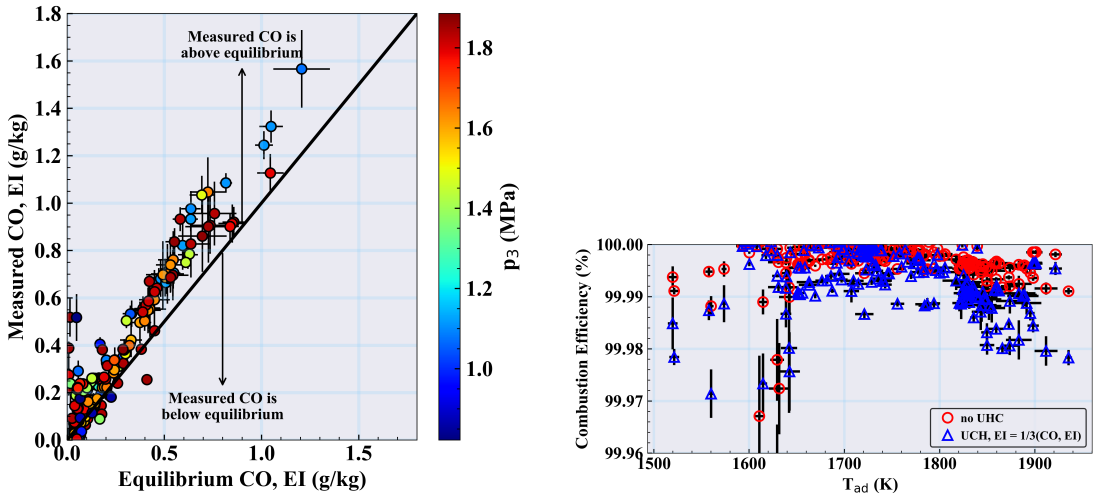

(a) *(b)*

Figure 9: *High power conditions: (??) comparison of measured and equilibrium CO emissions and (b) combustion efficiency.*

.

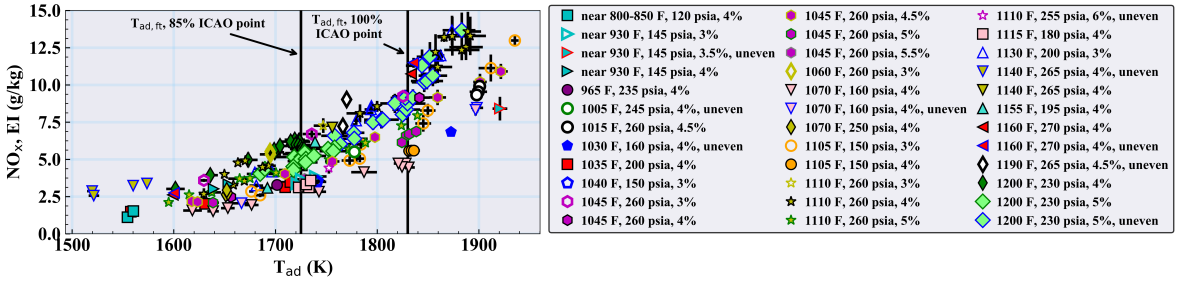

Figure 10: *NO_x emissions at high power conditions. Unless a curve is labeled "uneven", all stages have approximately the same fuel-air ratio.*

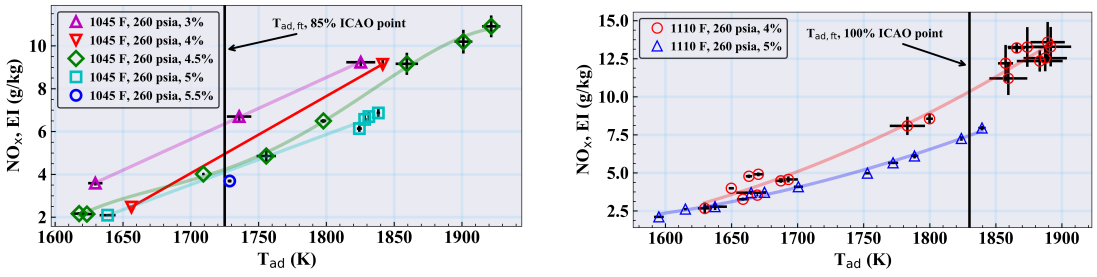

(a) *(b)*

Figure 11: *High power conditions: NO_x as a function of the adiabatic flame temperature T_{ad} at (a) 260 psia and 1045 F (b) 260 psia and 1110 F.*

.

Table 2: *Coefficients for correlation equations. For Fit 1, the values of a, b, and c are taken from Tacina et al, 2005.*[1]

Configuration	Fit	a	b	c	d_p	e_p	d_m	e_m	R^2
LDI-3-3	Fit 1	0.500	340	-0.600	1.12×10^{-3}	448	2.62×10^{-6}	173	0.915
LDI-3-3	Fit 2	0.931	234	-0.829	4.97×10^{-6}	246	7.36×10^{-7}	187	0.933

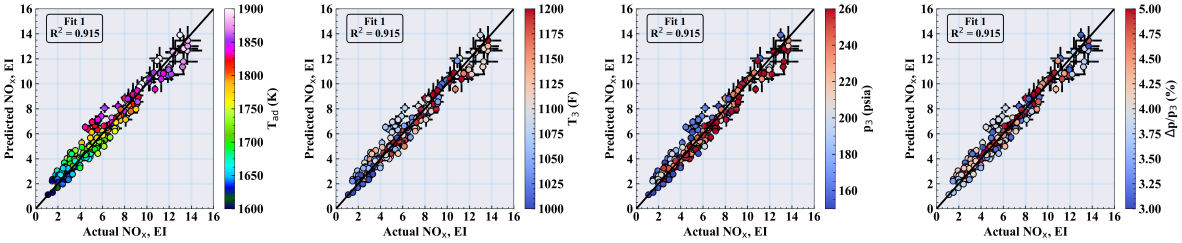

Figure 12: *NO_x emissions: predicted using Fit 1 vs measured values.*

and m refer to the pilot and main stages, respectively. The local adiabatic flame temperature is calculated separately for each stage, with $T_{\text{ad, p}}$ being the adiabatic flame temperature for the pilot stage and $T_{\text{ad, m1}}$, $T_{\text{ad, m2}}$, and $T_{\text{ad, m3}}$ being the adiabatic flame temperatures for stages main 1, main 2, and main 3.

Initially, the values for a, b, and c were taken from Tacina et al, 2005,[1] and an optimization was done on d_p, e_p, d_m, and e_m. This correlation equation is called "Fit 1" and the coefficients are given in the first row of Table 2. The R^2 value for this correlation was reasonable: 0.915. As would be expected with an R^2 value of 0.915, the NO_x predicted using Fit 1 matches the measured NO_x emissions reasonably well, as shown in Figure 12.

Using Fit 1, the NO_x emissions at 100% and 85% power are estimated to be 12.8 g/kg and 6.8 g/kg. For the ICAO landing and take-off (LTO) cycle, the NO_x severity parameter D_p/F_{00} is 12.32 g/kN — an 89% reduction with respect to the CAEP/6 standard.

However, Fit 1 may be underestimating NO_x emissions. The predicted NO_x at 100% power, 12.8 g/kg, is considerably lower than the rough estimate of 15-17 g/kg. In addition, a close examination of Figure 12 shows that there are systematic errors in Fit 1. Coloring each point by combustor inlet shows that NO_x is consistently under-predicted at the higher inlet pressures and over-predicted at the lower inlet pressures. This indicates that the calculated NO_x emissions are probably low at both 85% and 100% power. Looking at the graph where points are colored by adiabatic flame temperature further indicates that Fit 1 may be under-predicting NO_x emissions: NO_x is under-predicted at both the 85% power conditions (1725 K, 6-8 g/kg NO_x) and the 100% power conditions (1830 K, NO_x above 12 g/kg).

Therefore, a second correlation equation was found. This time, an optimization was done on all 7 parameters. This resulting correlation equation is called "Fit 2" and the coefficients are given in the second row of Table 2. The R^2 value for this fit is slightly better — 0.933 — and the plot of predicted versus measured NO_x (Figure 13 does not show the systematic errors of Fit 1.

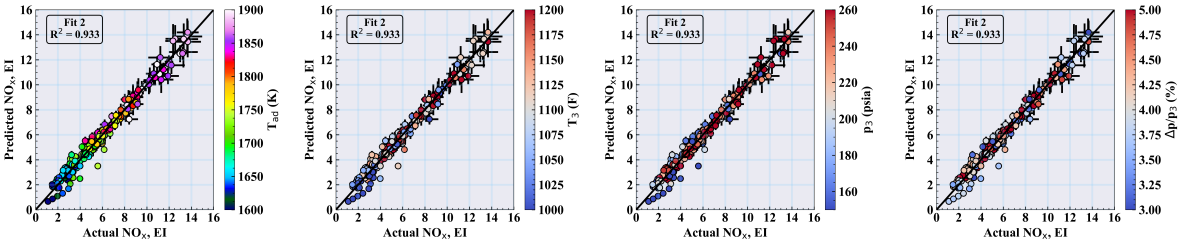

Figure 13: *NO_x emissions: predicted using Fit 2 vs measured values.*

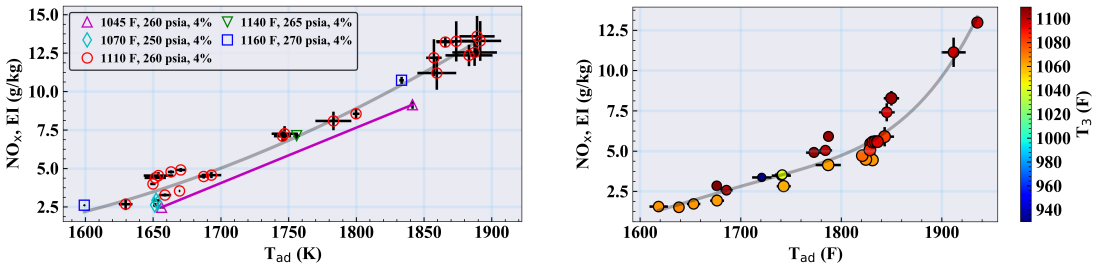

(a) *(b)*

Figure 14: *High power conditions: Effect of inlet temperature, T_3. Shown are (a) 260 psia and 4% air pressure drop and (??) a variety of conditions with inlet pressures near 150 psia.*

Using Fit 2, the NO_x emissions at 100% and 85% power are estimated to be 18.8 g/kg and 8.2 g/kg. For the ICAO LTO cycle, the NO_x severity parameter D_p/F_{00} is 15.03 g/kN — an 86% reduction with respect to the CAEP/6 standard.

Note the pressure exponent of 0.931 in Fit 2 is higher than the assumed pressure exponent of 0.5-0.6 used to make the rough estimate of NO_x emissions. The rough scaling used to estimate the NO_x emissions at the beginning of this section can be repeated, this time scaling with $p_3^{0.931}$. As stated above, Figures 10-14b give NO_x emissions of 10.5 g/kg and 5 g/kg when matching the 85% and 100% power conditions for all variables except pressure. Correcting for pressure, this time with $p_3^{0.931}$, yields estimates of NO_x emissions at 100% and 85% power to be 21.2 g/kg and 8.8 g/kg. For the ICAO LTO cycle, the NO_x severity parameter D_p/F_{00} is 15.97 — an 85% reduction with respect to the CAEP/6 standard.

D. Effect of inlet conditions

This section examines the effect on combustor inlet conditions on NO_x emisisons. Starting with the least important condition (T_3), this section primarily looks at pairs of NO_x vs. flame temperature curves that are matched in all conditions except one. The effect of each inlet condition is compared to what would be expected based on the correlation equation Fit 2.

1. Inlet temperature

The effect of inlet temperature is shown in Figure 14. Based on Fit 2, the effect of inlet temperature should be fairly small. For example, if the inlet temperature increases from 1045 to 1160 — as in Figure 14a — the NO_x emission index should increase only by 30%. Figure 14a does indeed show an approximately 30% increase in NO_x as the inlet temperature increases from 1045 F to 1160 F.

The data in Figure 14a was taken near the highest inlet pressure obtainable in CE-5 Stand 1, about 260 psia. Figure **??** shows the effect on inlet temperature near the lowest inlet pressure used for high-power points, 150 psia. Again, the effect of inlet temperature is small.

2. Air pressure drop

Figure 11 shows the effect of air pressure drop on NO_x emissions. Although increasing pressure drop does tend in general to decrease NO_x emissions, both figures show the effect of air pressure drop is inconsisent. For example, when comparing pressure drops of 3% and 4%, Figure 11a shows the difference between NO_x emissions *decreases* with increasing flame temperature. In contrast, when comparing pressure drops of 4% and 5%, both Figures 11a and 14b show the difference between NO_x emissions *increases* with increasing flame temperature. Due to this inconsistent effect of pressure drop, a simple term — $\Delta p^{-0.829}$ — cannot possibly capture the correct physics.

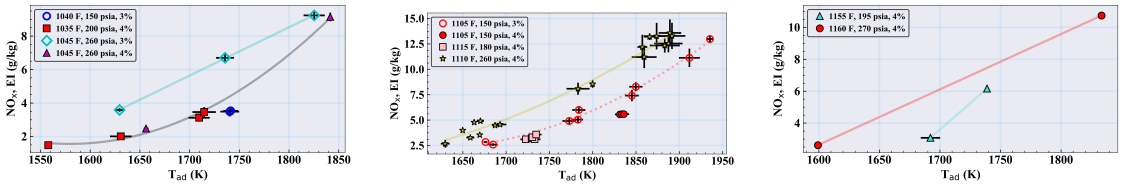

(a) *(b)* *(c)*

Figure 15: *High power conditions: Effect of inlet pressure, p_3. Shown are (a) 1040 F and 4% air pressure drop and (??) 1110 F and 4% pressure drop, and (c) 1160 F and 4% pressure drop.*

3. Inlet pressure

Figure 15 shows the effect of combustor inlet pressure on NO_x emissions. Increasing the combustor inlet pressure does in general tend to increase NO_x emissions. But, as with pressure drop, the effect is inconsistent. Fit 2 estimates the NO_x emissions increase with $p_3^{0.931}$. In some cases, this underestimates the effect of p_3 (Figure 15a, 3% curves, near T_textad=1740 K; Figure 15b). Other times, it overestimates the effect of p_3 (Figure 15a, 4% curves; Figure 15c). A simple power scaling for p_3 does not capture the correct physics.

4. Discussion of NO_x correlation equations

NO_x emissions are not a consistent function of inlet conditions. Therefore, simple correlation equations will not correctly estimate NO_x at all high power conditions.

A physics-based approach to developing NO_x correlation equations could be more accurate. Estimating the thermal NO_x based on physics requires knowledge of the NO_x formation rate, the volume/area, and the time/flowrate. In turn, estimating the NO_x formation rate requires knowledge of the: local, instantaneous O_2 concentration; local, instantaneous temperature; N_2 concentration.

Estimating these quantities is not trivial. However, following the approch taken by Hsieh et al[9] for industrial gas burners, it may be possible to estimate these quantities by dividing the flame into multiple zones, each with a different scaling. For LDI combustors, reasonable zones might be a high-temperature, low-volume, intense flame zone; an intermediate-temperature, medium-volume recirculation/low velocity zone; and a lower-temperature, high-volume post-flame zone. Both optical diagnostics and CFD show high-temperature flame regions followed by a lower-temperature post-flame zone.

Furthermore, high-speed flame luminosity measurements and time-accurate CFD show that the instantaneous flame location varies significantly with time. For example, flame luminosity measurements of LDI-1 designs show that in the primary flame zone the RMS is on the order of half the mean. Therefore, when dividing the flame into the intense flame zone and the recirculation zone, the physical location may be the same for both zones; time-accurate CFD and optical diagonostics measurements could be used to estimate what fraction of the time a given location should be considered an intense flame zone and what fraction of time an intermediate-temperature recirculation zone.

E. Comparison with LDI-2

Figure 16 compares NO_x emissions for LDI-3 to the LDI-2 configurations. Levels of NO_x emissions for LDI-3 are similar to those of the three LDI-2 configurations. The largest difference is the slope of the NO_x vs. flame temperature curve: it tends to be steeper for LDI-3 than for LDI-2; LDI-3 tends to have lower NO_x emissions than LDI-2 at lower flame temperatures and similar or higher NO_x emissions at higher flame temperatures.

F. Supersonic cruise emissions

Figure 17 shows NO_x emissions near the supersonic PC90 cruise conditions: a T_3 of 1226 F, a p_3 of 220 psia, and an equivalence ratio of 0.43. This test condition challenged the capabilities of CE-5 Stand 1 and the combustor hardware. Although CE-5 Stand 1 could reach p_3 and came near to reaching T_3, it could not reach the desired equivalence ratio when adjusted for 15%-20% liner cooling. There were two reasons the

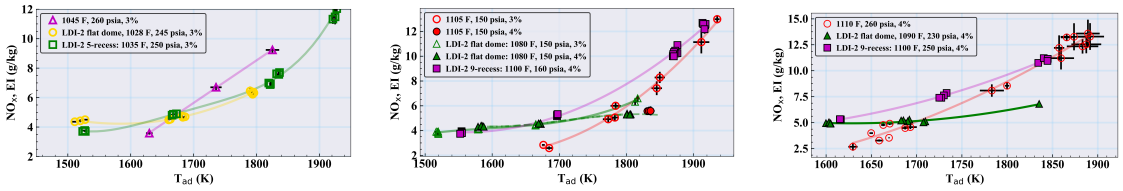

(a) *(b)* *(c)*

Figure 16: *High power conditions: Comparison with LDI-2 configurations. (a) 1045 F and 260 psia, (b) 1100 F and 150 psia, and (c) 1110 F and 260 psia.*

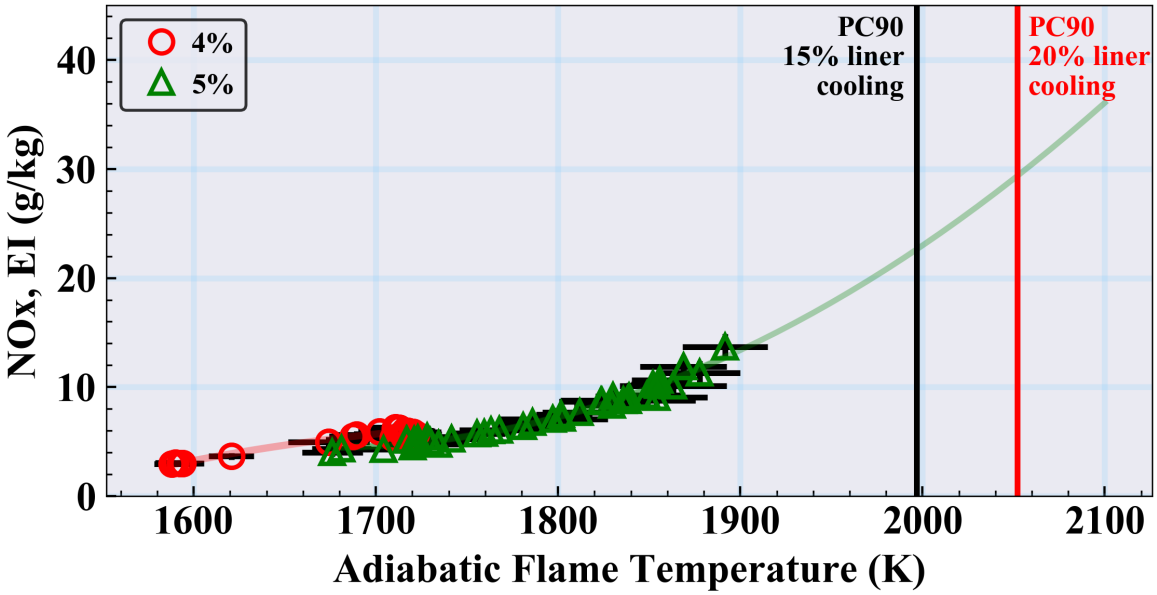

Figure 17: *NO_x emissions at supersonic cruise conditions. This data was taken at an inlet temperature of 1200 F and an inlet pressure of 230 psia.*

desired equivalence ratio could not be reached. First, the combustor dome temperature neared its limits. To reduce the dome temperature, the air pressure drop was increased and the fuel staging was changed to minimize dome temperature instead of NO_x emissions. Changing the air pressure drop and fuel staging allowed for higher equivalence ratios. But then we encountered a second problem: the burnt gas temperature in the flametube was too high. To reach the desired equivalence ratios, a higher-temperature ceramic casting for the flametube liner and perhaps additional quench cooling water would be needed.

Therefore, estimating the NO_x emissions at supersonic cruise required an extrapolation for flame temperature. Using a second-order univariate spline to extrapolate the 5% pressure drop curve, supersonic cruise NO_x emissions are estimated to be 23 g/kg with 15% liner cooling and 29 g/kg with 20% liner cooling. These estimates are well above the supersonic program goal of 5 g/kg.

IV. Summary

This paper presents gaseous emissions results from flametube tests of a low-NO_x aircraft gas turbine engine combustor concept. The low-NO_x combustor concept is a third-generation swirl-venturi lean direct injection (SV-LDI-3) design. It was developed to meet the NASA Advanced Air Transport Technology project goals: the development of a combustor suitable for a small-core engine with NO_x emissions 80% below the CAEP/6 standard. As far as was possible, emissions were evaluated at the ICAO points. However, the CE-5 Stand 1 flametube could not reach the combustor inlet pressure for the 85% and 100% power points.

Therefore, correlation equations were developed to estimate NO_x emissions. These correlation equations gave an estimated NO_x reduction of 85%-89% with respect to CAEP/6, exceeding project goals.

Acknowledgments

Woodward, FST, provided the combustor hardware under a Space Act Agreement. NASA's Advanced Air Transport Technology (AATT) project supported flametube testing in NASA's CE-5 medium pressure flametube.

Thanks to the engineering and technician staff for NASA's CE-5 test rig.

Thanks also to the open-source sofware community for providing the software used for data analysis: numpy,[10] matplotlib,[11] pandas,[12] and ipython.[13]

References

[1]Tacina, R., Lee, P., and Wey, C., 2005. A lean-direct-injection combustor using a 9 point swirl-venturi fuel injector. ISABE-2005-1106.

[2]Tacina, K. M., Lee, P., Mongia, H., Chang, C. T., He, Z., and Dam, B., 2014. A second generation swirl-venturi lean direct injection combustion concept. AIAA 2014-3434.

[3]Tacina, K. M., Lee, P., Mongia, H., He, Z., Podboy, D. P., and Dam, B., 2016. A comparison of three second-generation swirl-venturi lean direct injection combustor concepts. AIAA 2016-xxxx.

[4]SAE E-31 Technical Committee, 2011. Procedure for the continuous sampling and measurement of gaseous emissions from aircraft turbine engines. SAE ARP 1256D.

[5]SAE E-31 Technical Committee, 2013. Procedure for the analysis and evaluation of gaseous emissions from aircraft engines. SAE ARP 1533B.

[6]McBride, B., and Gordon, S., 1992. Computer program for calculating and fitting thermodynamic functions. NASA RP-1271.

[7]McBride, B., Zehe, M., and Gordon, S., 1993. NASA Glenn coefficients for calculating thermodynamic properties of individual species. NASA TP-3287.

[8]Tacina, K. M., Lee, P., Chang, C., He, Z., Dam, B., and Podboy, D., 2015. An assessment of combustion dynamics in a low-no$_x$ second-generation swirl-venturi lean direct injection combustion concept. ISABE-2015-20249.

[9]Hsieh, T.-C. A., Dahm, W. J., and Driscoll, J. F., 1998. "Scaling laws for NO_x emission performance of burners and furnaces from 30 kw to 12 mw". *Combustion and Flame,* ***114***, pp. 54–80.

[10]Walt, S. v. d., Colbert, S. C., and Varoquaux, G., 2011. "The numpy array: A structure for efficient numerical computation". *Computing in Science and Engineering,* ***13***(2), pp. 22–30.

[11]Hunter, J. D., 2007. "Matplotlib: A 2d graphics environment". *Computing In Science & Engineering,* ***9***(3), pp. 90–95.

[12]McKinney, W., 2010. "Data structures for statistical computing in python". In Proceedings of the 9th Python in Science Conference, S. van der Walt and J. Millman, eds., pp. 51 – 56.

[13]Pérez, F., and Granger, B. E., 2007. "IPython: a system for interactive scientific computing". *Computing in Science and Engineering,* ***9***(3), May, pp. 21–29.